Published online 25 August 2017 *Nucleic Acids Research, 2017, Vol. 45, No. 18* **10693–10705**
doi: 10.1093/nar/gkx740

The Cdc45/RecJ-like protein forms a complex with GINS and MCM, and is important for DNA replication in *Thermococcus kodakarensis*

Mariko Nagata[1], Sonoko Ishino[1,*], Takeshi Yamagami[1], Hiromi Ogino[1], Jan-Robert Simons[2], Tamotsu Kanai[2], Haruyuki Atomi[2] and Yoshizumi Ishino[1,*]

[1]Department of Bioscience and Biotechnology, Graduate School of Bioresource and Bioenvironmental Sciences, Kyushu University, Fukuoka, Fukuoka 812-8581, Japan and [2]Department of Synthetic Chemistry and Biological Chemistry, Graduate School of Engineering, Kyoto University, Kyoto, Kyoto 615-8510, Japan

Received June 03, 2017; Revised August 09, 2017; Editorial Decision August 10, 2017; Accepted August 12, 2017

ABSTRACT

The archaeal minichromosome maintenance (MCM) has DNA helicase activity, which is stimulated by GINS in several archaea. In the eukaryotic replicative helicase complex, Cdc45 forms a complex with MCM and GINS, named as CMG (Cdc45-MCM-GINS). Cdc45 shares sequence similarity with bacterial RecJ. A Cdc45/RecJ-like protein from *Thermococcus kodakarensis* shows a bacterial RecJ-like exonuclease activity, which is stimulated by GINS *in vitro.* Therefore, this archaeal Cdc45/RecJ is designated as GAN, from GINS-associated nuclease. In this study, we identified the CMG-like complex in *T. kodakarensis* cells. The GAN·GINS complex stimulated the MCM helicase, but MCM did not affect the nuclease activity of GAN *in vitro*. The gene disruption analysis showed that GAN was non-essential for its viability but the Δ*gan* mutant did not grow at 93°C. Furthermore, the Δ*gan* mutant showed a clear retardation in growth as compared with the parent cells under optimal conditions at 85°C. These deficiencies were recovered by introducing the *gan* gene encoding the nuclease deficient GAN protein back to the genome. These results suggest that the replicative helicase complex without GAN may become unstable and ineffective in replication fork progression. The nuclease activity of GAN is not related to the growth defects of the Δ*gan* mutant cells.

INTRODUCTION

Chromosomal DNA replication is an essential process for cell proliferation. A series of highly regulated events occurs during DNA replication, from initiation to termination, to maintain a constant level of genetic material (1). The molecular mechanisms of DNA replication have been studied in a variety of organisms in the three domains of life, from Bacteria, Eukarya and Archaea (reviewed in (1–3)). One of the key proteins involved in the initiation and elongation processes of DNA replication is the helicase. The minichromosome maintenance (MCM) is the helicase core complex in Eukarya and Archaea, whereas the bacterial helicase is DnaB. Eukaryotic MCM consists of Mcm2–7 and forms a hexameric complex, and GINS and Cdc45 are required to form the CMG (Cdc45·MCM·GINS) complex to exert the helicase activity *in vitro*. The Cdc45 protein was originally found, with an unknown function, in the pre-replication complex (pre-RC) in *Saccharomyces cerevisiae* (4) and now is proposed to move with the replication fork. The components of the GINS complex, consisting of four different proteins, Sld5, Psf1, Psf2 and Psf3, were also originally identified in *S. cerevisiae* as essential protein factors for the initiation of DNA replication (5). MCM, Cdc45 and GINS exist as a complex in *Xenopus* egg extracts, as originally demonstrated by immunoprecipitation experiments (6). Subsequently, the CMG complex was isolated from yeast (7), *Drosophila* (8) and *Xenopus* egg extracts (9). Biochemical and structural studies of the eukaryotic CMG complex are now actively progressing (10–17). Cdc45 and GINS perform structural roles to facilitate the formation of the active helicase complex by MCM.

Most archaeal organisms contain only a single Mcm homolog (18). The homohexameric MCM exhibits distinct DNA helicase activity *in vitro*, but the helicase activity is stimulated by the interaction with GINS in several archaea (19–23). A detailed sequence analysis revealed that the eukaryotic Cdc45 protein possesses a DHH phosphodiesterase domain, which is also present in bacterial RecJs (24). The RecJ protein is considered to function in

*To whom correspondence should be addressed. Tel: +81 92 642 4217; Fax: +81 92 642 3085; Email: ishino@agr.kyushu-u.ac.jp
Correspondence may also be addressed to Sonoko Ishino. Tel: +81 92 642 4218; Fax: +81 92 642 3085; Email: sonoko@agr.kyushu-u.ac.jp
Present address: Hiromi Ogino, Faculty of Engineering, Gifu University, 1-1 Yanagido, Gifu 501–1193, Japan.

DNA repair pathways, including homologous recombination, base excision repair and mismatch repair, as a 5′–3′ single-stranded DNA (ssDNA) specific exonuclease in bacterial cells (25–27). However, no nuclease activity has been detected for eukaryotic Cdc45 so far. The Cdc45/RecJ-like proteins are also found in Archaea, supporting the notion that they are homologs (24,28). In addition, a Cdc45/RecJ-like protein from the hyperthermophilic archaeon, *Thermococcus kodakarensis,* has a 5′–3′ single-stranded DNA (ssDNA)-specific exonuclease activity, as in the bacterial RecJs and this nuclease activity is stimulated by GINS *in vitro* (29). Therefore, this archaeal protein was designated as GAN, from GINS-associated nuclease. Investigations of the similarities and differences between the archaeal Cdc45/RecJ proteins and those from other domains are interesting research subjects.

The formation of a complex of the Cdc45/RecJ-like protein with MCM and GINS from *Sulfolobus* species, which are hyperthermophiles from crenarchaea, was recently demonstrated (30). The association of Cdc45/RecJ with GINS and MCM robustly stimulated the helicase activity, although GINS had no effect on the helicase activity of MCM as previously shown (31). Cdc45/RecJ by itself did not show any detectable effect on the MCM helicase activity. This report indicated that the CMG complex is the central component of the replicative helicase in *Sulfolobus.* We also reported the CMG-like complex in *Thermoplasma acidophilum,* in which the Cdc45/RecJ-like protein is one of two homologs, RecJ1 and RecJ2. The CMG-like complex consists of Mcm, Gins51 (homotetramer) and RecJ2 in this archaeon, and RecJ2 showed 3′–5′ but not 5′–3′, exonuclease activity *in vitro* (32).

T. kodakarensis has three *mcm* homologs, but only one of them, *mcm3*, is essential for its viability and thus the MCM3 complex should be the replicative helicase core in the cells (20,33). Furthermore, GINS stimulates the helicase activity of MCM3 (20). We solved the crystal structure of the *T. kodakarensis* GINS complex, consisting of Gins51 and Gins23 with a 2:2 ratio, which revealed its striking structural similarity to the human GINS assembly, with remarkable differences in the C-terminal B domain of Gins51 (34). Furthermore, we reported the crystal structure of *T. kodakarensis* GAN, which is similar to the bacterial RecJs from *Thermus thermophilus* and *Deinococcus radiodurans* with strict conservation of the catalytic residues (35). This result indicated that the molecular mechanism of the exonuclease function of GAN is the same as that of bacterial RecJ. In contrast, a eukaryotic study demonstrated that GAN and eukaryotic Cdc45 share a domain called CID, from CMG-Interaction Domain (36), which probably functions for activating MCM. We also determined the crystal structure of GAN in complex with the C-terminal domain of Gins51C, which is bound to the N-terminal domain of GAN (35). This structure is comparable to that observed in the cryo-EM structure of the eukaryotic CMG complex (15,16). From the structural feature of GAN, which has both characteristic structures for bacterial RecJ and eukaryotic Cdc45, it is expected that the archaeal GAN may have dual roles as an exonuclease in DNA repair and a CMG component in DNA replication. On the other hand, a report was published recently describing the function of the GAN nuclease for the removal of primers during Okazaki fragment maturation in the lagging strand synthesis, based on genetic analyses of the *gan*-deletion mutant in *T. kodakarensis* (37). This report revealed that either Fen1 or GAN can be deleted with no discernible effects on viability and growth, but the double mutant of these genes could not be isolated. Based on these genetic analyses, the authors proposed that GAN and Fen1 work in the same step, to remove primers from the Okazaki fragment.

To elucidate the function of the Cdc45/RecJ/GAN protein in an archaeon, we investigated the interactions of GAN with MCM3 and GINS in *T. kodakarensis* cells and found that the CMG-like complex is also formed in these archaeal cells. Moreover, a *gan*-deletion mutant (Δ*gan*) strain was isolated independently from *T. kodakarensis*. The *gan*-deletion mutant showed a temperature-sensitive phenotype and moreover, a clear growth retardation as compared with the parental cells under optimal conditions. These results suggest that the archaeal Cdc45/RecJ is non-essential for viability, but still plays an important role. The Δ*gan* mutation may affect replication fork progression.

MATERIALS AND METHODS

Recombinant protein purification

The recombinant MCM3 (TK_RS08085), GAN (TK_RS06185) and GINS (Gins51: TK_RS02640, Gins23; TK_RS08080) proteins were prepared according to the procedures described in our previous reports (20,34–35). Briefly, GAN (wild-type (WT) and D36A) and GINS were overproduced in *Escherichia coli* BL21-CodonPlus (DE3)-RIL cells (Agilent Technologies). The proteins were purified by heat treatment at 80°C for 20 min and sequential chromatographies on HiTrap Phenyl HP (GE Healthcare) and HiTrap Q HP (GE Healthcare) columns. GAN-D36A was prepared in the same manner as the WT protein. HiTrap Heparin HP (GE Healthcare) was additionally used for the purification of MCM3. The purified proteins were quantified by measuring the absorbance at 280 nm, with theoretical extinction coefficients of 34380, 216720 and 76780 M^{-1} cm^{-1} for GAN, MCM3 (homohexamer) and GINS (heterotetramer), respectively, based on tryptophan and tyrosine contents (38). MCM3 is referred to as MCM hereafter in this work.

Site-specific mutagenesis

To construct the expression plasmid using pET-21a(+) (Novagen) for GAN-D36A and the plasmid to replace the native *gan* gene with *gan-D34A/D36A*, PCR-mediated mutagenesis was performed with a QuikChange™ site-directed mutagenesis kit (Agilent Technologies). The templates were pET-GAN (35) and pUD3-GAN (described below). The designed mutations were confirmed by nucleotide sequencing. The primers used for each mutagenesis are shown in Supplementary Table S1.

Exonuclease assay

Oligonucleotides used as the DNA substrates were obtained from Hokkaido System Science and Sigma-Aldrich, and

are listed in Supplementary Table S2. The combinations of oligonucleotides for the substrates are shown in Supplementary Table S3. The annealing of the appropriate oligonucleotides were performed in 20 mM Tris–HCl, pH 7.5 and 50 mM NaCl. The nuclease reaction of GAN was performed in mixtures (20 μl), containing 25 mM Bis–Tris, pH 7.0, 125 μg/ml bovine serum albumin (BSA), 1 mM DTT, $MnCl_2$ or $MgCl_2$, FITC-labeled DNA substrates and various concentrations of the recombinant proteins. The reaction mixture was pre-incubated for 3 min without metal ions. The reaction was started by adding $MnCl_2$ or $MgCl_2$ and terminated by adding 5 μl of stop solution A (12.5% Ficoll, 100 mM EDTA, 0.05% bromophenol blue and 0.05% xylene cyanol) for native polyacrylamide gel electrophoresis (PAGE) or adding an equal volume of stop solution B (98% formamide, 10 mM EDTA, 0.01% bromophenol blue and 0.01% xylene cyanol) for denaturing PAGE and immediately transferred onto ice. The gel images were visualized by using a Typhoon Trio+ (GE Healthcare) image analyzer. Further modifications of the reaction and PAGE conditions are described in the respective sections.

Surface plasmon resonance (SPR) analysis

The Biacore J system (GE Healthcare) was used to examine the physical interactions of GAN–GINS, GAN–MCM and GINS–GAN–MCM. Either GAN or Gins51 was fixed on a CM5 sensor Chip (GE Healthcare), according to the manufacturer's recommendations. The Gins51-chip was the same as that used in our previous analysis (34). The GINS-chip was prepared by applying the Gins23 protein to the Gins51-chip until saturation was achieved. The purified GINS, GAN and MCM proteins, in running buffer (10 mM HEPES–NaOH, pH 7.4, 150 mM NaCl, 3 mM EDTA and 0.2% Tween 20), were applied for 120 s to the protein-immobilized chips, at a flow rate of 30 μl/min at 25°C. The bound analytes were removed by the regeneration buffer (10 mM HEPES–NaOH, pH 7.5, 1 M NaCl and 0.2% Tween 20) at the end of each cycle. The apparent equilibrium constants (K_D) of the interactions of (GAN-immobilized GAN·GINS)–MCM and (GINS-immobilized GAN·GINS)–MCM were determined from the association and dissociation curves of the sensorgrams, using the BIAevaluation program (GE Healthcare).

Strains and culture conditions

T. kodakarensis KUW1 (Δ*pyrF*, Δ*trpE*) (39) was used as the parental host strain for mutant construction. *T. kodakarensis* cells were cultivated under anaerobic conditions at 85 or 93°C in either nutrient-rich medium (ASW-YT or MA-YT) or synthetic medium (ASW-AA), in basically the same manner as previously described (40–42). ASW-YT medium was composed of 0.8 × artificial seawater (43), 5.0 g/l yeast extract (Difco) and 5.0 g/l tryptone (Difco), supplemented with sodium pyruvate (5.0 g/l) or elemental sulfur (5.0 g/l) (ASW-YT-Pr or ASW-YT-S^0, respectively). For large-scale cultivation, 30.2 g/l artificial sea salts (Marine Art SF; Tomita Pharmaceutical, Naruto, Japan) were used instead of ASW (MA-YT-Pr). The minimal ASW-AA medium, which supported the growth of strain KUW1 and the solid medium were prepared as previously described (40,41). To select transformants with 5-FOA resistance, 10 g/l 5-fluoroorotic acid (5-FOA) and 60 mM NaOH were added to the solid medium.

Immunoprecipitation assay

T. kodakarensis KOD1 cells were cultured in 2 l of MA-YT-Pr medium at 85°C, and harvested at the late exponential phase by centrifugation for 10 min at 5000 × *g*. The cells (9.1×10^{11} cells) were resuspended in 45.5 ml of 50 mM Bis–Tris buffer, pH 7.0, to a final concentration of 2×10^{10} cells/ml and were disrupted by sonication. The cell extracts were obtained by centrifugation for 10 min at 23 000 × *g*. Polyclonal anti-MCM, anti-Gins51, anti-Gins23 and anti-GAN antisera were raised independently, by immunizing rabbits with the purified recombinant proteins as antigens. A 20 μl portion of rProtein A Sepharose FF (GE Healthcare) was washed three-times with phosphate buffered saline-Tween 20 (PBS-T: 10 mM sodium phosphate, pH 7.5, 150 mM NaCl and 0.1% Tween 20), mixed with 500 μl PBS-T containing 100 μl of each antiserum and incubated on a rotating wheel at room temperature for 1 h. Each mixture was washed three-times with 500 μl of 0.2 M triethanolamine, pH 8.0. Each antibody was cross-linked to the rProtein A Sepharose with 10 mM dimethyl sulfide (Thermo Fisher Scientific), according to the manufacturer's protocol. After equilibration of the antibody-conjugated rProtein A Sepharose with 50 mM Bis–Tris, pH 7.0, a 7.5 ml aliquot of the cell extract was added. The mixture was incubated on a rotating wheel at room temperature for 1 h. The precipitates were washed three-times with 50 mM Bis–Tris, pH 7.0 and the immunoprecipitated proteins were eluted with 75 μl of gel-loading solution, containing 50 mM Tris–HCl, pH 6.8, 10% glycerol, 5% β-mercaptoethanol, 0.2% bromophenol blue and 2% SDS. The eluted proteins were separated by SDS-PAGE, followed by western blot analysis.

Western blot analysis

The proteins on the gel were electroblotted onto a polyvinylidene difluoride (PVDF) membrane (Bio-Rad) using a Trans-Blot Turbo Transfer System (Bio-Rad) and reacted with the anti-MCM, anti-GAN, anti-Gins51 and anti-Gins23 antisera, prepared by each recombinant protein. Anti-Rabbit IgG HRP (Rabbit TrueBlot, Rockland Immunochemicals, Inc.) was used as the secondary antibody. The proteins were visualized by an enhanced chemiluminescence system (Millipore) and images were obtained and quantified with an LAS-3000 image analyzer (Fujifilm).

Helicase assay

The substrate DNA was prepared as described in the section of exonuclease assay. The helicase activity of MCM with trap DNA was measured in a 20 μl reaction mixture, containing 25 mM Bis–Tris, pH 7.0, 50 mM NaCl, 5 mM $MgCl_2$, 1 mM DTT, 125 μg/ml BSA, 2.5 mM adenosine triphosphate (ATP), 50 nM DNA substrate, 150 nM trap DNA (to prevent re-annealing of the unwound DNA),

250 nM MCM (as the hexamer) and 2 μM GINS (as the tetramer), with increasing amounts of GAN (WT or D36A). After an incubation for 30 min at 65°C, the reactions were terminated by adding 5 μl of 5 × stop solution C (12.5% Ficoll, 100 mM EDTA, 0.5% SDS and 0.1% Orange G) and immediately transferred onto ice. The samples were separated by 10% PAGE in TBE (89 mM Tris, 89 mM boric acid and 2.5 mM EDTA, pH 8.3). The helicase activity of MCM with replication protein A (RPA) was measured in a 20 μl reaction mixture, containing 25 mM Bis–Tris, pH 7.0, 50 mM NaCl, 5 mM $MgCl_2$, 1 mM DTT, 125 μg/ml BSA, 2.5 mM ATP, 50 nM DNA substrate and 250 nM MCM (as the hexamer), with 170 nM RPA, 0–4 μM GAN and 0–2 μM GINS (as the tetramer). After an incubation for 30 min at 65°C, the reactions were terminated by adding 5 μl of 5 × stop solution D (12.5% Ficoll, 100 mM EDTA and 0.1% Orange G) and immediately transferred onto ice. The samples were separated by 5.5% PAGE in 0.1 × TAE (4 mM Tris–acetate, 0.1 mM EDTA).

ATPase assay

The reaction mixtures (50 μl), containing 25 mM Bis–Tris, pH 7.0, 50 mM NaCl, 5 mM $MgCl_2$, 2.5 mM ATP, 1 mM DTT and 0.1 μM MCM (as the hexamer) were incubated for 10 and 20 min at 70°C in the presence or absence of 40 μM (in nucleotides) DNA (M13mp18 ssDNA or M13mp18 RF DNA). The effects of GAN and GAN·GINS were analyzed by the addition of 0–1 μM GAN and 0–0.5 μM GINS (as the tetramer) to the reaction. The amounts of orthophosphate produced in the reactions were analyzed with an EnzChek Phosphate Assay kit (Thermo Fisher Scientific), according to the manufacturer's protocol. The standard error of the mean (SEM) was calculated from three independent experiments.

Construction of the *T. kodakarensis* Δ*gan* and Δ*gan::gan-D34A/D36A* strains

The *gan* gene, along with 1000 bp of its 5′- and 3′-flanking regions, was amplified from *T. kodakarensis* genomic DNA, using the primer sets fgan-F/R (Supplementary Table S4). The PCR fragment was inserted into pUD3 (44) after digestion with BamHI and EcoRI, and the resultant plasmid was designated as pUD3-GAN. An inverse PCR to remove the *gan*-encoding region was performed, using the dgan-F/R primer set and the amplified fragment was self-ligated (pUD3-ΔGAN). The sequences of the 5′- and 3′-flanking regions were confirmed. The transformation was performed as described previously (44). The genotypes of the isolated transformants were analyzed by PCR, using gan-F/R and fgan-F/R, and the *gan* gene locus of the candidate strains was sequenced to confirm the gene disruption. The plasmid bearing the gene encoding GAN-D34A/D36A (pUD3-GAN-D34A/D36A) was prepared by site-specific mutagenesis. The Δ*gan* strain was transformed with pUD3-GAN-D34A/D36A and the strain harboring the nuclease-deficient *gan* gene was isolated in the same manner and designated Δ*gan::gan-D34A/D36A*.

Growth measurements

The growth characteristics of the *T. kodakarensis* strains KUW1, Δ*gan* and Δ*gan::gan-D34A/D36A* were measured, as follows. Each strain was pre-cultured in ASW-YT-Pr medium at 85°C for 6–12 h, until the culture attained an OD_{660} of 0.2–0.3. After pre-culturing, the cells were inoculated into 15 ml of ASW-YT-Pr to produce an OD_{660} of 0.01 and cultured at 85 and 93°C in glass test tubes. Cell densities were measured at appropriate intervals at 660 nm (OD_{660}), with a Novaspec II spectrophotometer (Pharmacia Biotech). Each strain was analyzed in duplicate and the measurements were performed three-times independently.

Drop dilution assay

The *T. kodakarensis* KUW1 and Δ*gan* strains were cultivated anaerobically at 85°C for 12 h, in ASW-YT-Pr medium. The cultures (6×10^8 cells/ml) were serially diluted 10-fold with 0.8 × ASW. The diluted cultures were spotted on ASW-YT plates and some of them were irradiated with an acrylic-filtered Ultraviolet (UV) lamp (Kenis) (wavelength 254 nm, 11 J/m^2, calculated by UV counter ATV-3W, ATTO). The plates were incubated anaerobically at 85 or 93°C for 20 h and the living cells were visualized by staining with Coomassie Brilliant Blue, after transfer to a PVDF membrane, as described previously (45). Experiments were performed in duplicate each time and repeated three-times independently.

Quantitative real-time PCR (qPCR)

The qPCR was performed according to the MIQE guidelines (46). The primers used for reverse transcription (RT) and qPCR are listed in Supplementary Table S5. The *T. kodakarensis* KUW1 and Δ*gan* strains were grown in 15 ml of ASW-YT-Pr medium, at 85 or 93°C. Cells in the log phase ($OD_{660} = 0.2$) were collected by centrifugation (4000 × *g*, 10 min). Total RNA was obtained with an RNeasy Mini kit with the RNase-free DNase Set (QIAGEN), according to the manufacturer's instructions. The cDNA was synthesized from 100 ng of total RNA, using the PrimeScript® RT reagent Kit with gDNA Eraser (Perfect Real Time) (Takara Bio). qRT-PCR was performed using SYBR® Premix Ex Taq™ II (Tli RNaseH Plus) and a Thermal Cycler Dice Real Time System Lite (Takara Bio). The RT of the predicted operon (*rps15, gan, pcc1* and *rps3:* TK_RS06180–TK_RS06195) was performed using the TK1254rps3-R primer, followed by PCR with the TK1251rps15-F/TK1254rps3-R primer set. The primers used for qPCR to amplify the 16S rRNA (reference gene), *gapdh* (reference gene) and *gan, pcc1*, *s3*, *gins51*, *gins23* and *mcm3* genes were TK16S-F/R, TK0765gapdh-F/R, TK1252gan-F/R, TK1253pcc1-F/R, TK1254rps3-F/R, TK0536gins51-F/R, TK1619gins23-F/R and TK1620mcm3-F/R, respectively, designed by using the open-source Primer3 software (47). The cycling conditions for all qPCR reactions were as follows: an initial denaturation step (one cycle of 95°C for 30 s); PCR (40 cycles of 95°C for 5 s and 60°C for 30 s); and a dissociation step (one cycle of 95°C for 15 s, 60°C for 30 s and 95°C for 15 s), to confirm the correct amplification of

the corresponding mRNAs. Samples were defined as negative if the Ct values exceeded 30 cycles. The data were analyzed using the ΔΔCt method. The mRNA levels were normalized to the 16S rRNA, *gapdh* or total mean expression level of each duplicated experiment. Three independent experiments were performed.

Quantitative elemental analysis for metals in *T. kodakarensis* cells

T. kodakarensis KOD1 cells were cultured in MA-YT-Pr, at 85°C for 10 h. The cells were harvested and the pellet was washed four-times with a >10-fold volume of a 0.3 M NaCl aqueous solution, to avoid carry-over of the materials from the medium (<0.001%). The pellet from 6.6×10^{10} cells corresponded to 1 g of the solid sample. The liquid sample was prepared from 1.6×10^{11} cells, disrupted in 12 ml of 20 mM Tris–HCl, pH 8.0 by sonication and centrifugation. The quantitative elemental analysis was conducted with an A-kit, Inc. (Ogaki, Japan). Briefly, the sample was treated with nitric acid and hydrogen peroxide for microwave digestion. For the manganese measurement, the solution was treated with a chelating agent. The concentrations of magnesium and manganese were measured with an inductively coupled plasma mass spectrometer (ICP-MS) (7700X, Agilent Technologies) and by inductively coupled plasma emission spectrometry (ICP-AES) (SPECTROBLUE TI, SPECTRO). *T. kodakarensis* cells are irregular cocci with a diameter of 1–2 μm (41) and therefore, the cell volume was estimated as a sphere with a 1.5 μm diameter, to calculate the intracellular concentrations of magnesium and manganese.

RESULTS

Physical interactions of GAN, GINS and MCM

The physical interactions of GAN–GINS (29,35) and GINS–MCM (20) were previously reported. The critical interest in the function of GAN is whether this RecJ/Cdc45-like protein participates in the replicative helicase complex in archaeal organisms. To answer this question, SPR analyses were performed using the highly purified GAN, GINS and MCM proteins (Figure 1A). The sensorgram of the GINS interaction with the GAN-immobilized chip reached a plateau in a few seconds and dissociation was not detected in the running buffer (after a 120 s injection) (Figure 1B). This result indicates a remarkably strong interaction between the two proteins. In contrast, MCM did not bind to the GAN-immobilized chip. MCM bound only after GINS binding to the GAN-immobilized chip, suggesting that GAN and MCM can exist in the same complex via GINS *in vitro*. The apparent K_D of GAN–GINS and MCM, calculated from the injections of various concentrations of MCM, was 1.9×10^{-7} M (Supplementary Figure S1A). Using the GAN bound to the GINS-immobilized chip, serially diluted MCM was loaded onto the chip and its association with the GAN·GINS complex was detected (Supplementary Figure S1B). The apparent K_D value calculated from this experiment was 1.8×10^{-7} M, which is also consistent with the results from the GAN-immobilized chip described above.

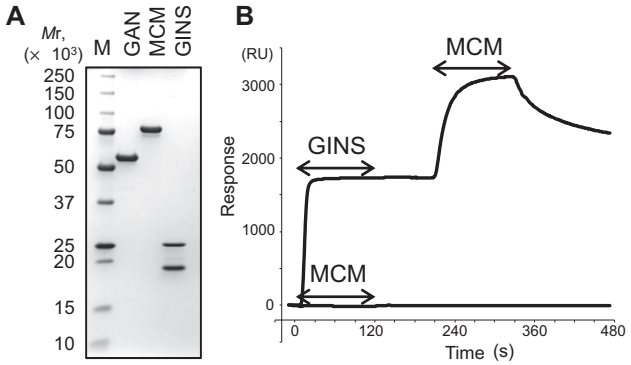

Figure 1. Physical interactions among GAN, GINS and minichromosome maintenance (MCM). (**A**) Purified recombinant proteins were analyzed by Sodium dodecylsulphate-polyacrylamide gel electrophoresis (SDS-PAGE). Purified GAN (1 μg), Mcm (1 μg) and GINS (Gins51 and Gins23) (1 μg) were subjected to SDS -10% PAGE followed by Coomassie Brilliant Blue staining. Protein size markers were run in lane M and their sizes are indicated on the left side of the gel. (**B**) SPR analyses for protein–protein interactions. MCM (2 μM as the hexamer) was loaded onto the GAN-immobilized chip for 120 s (lower sensorgram). GINS (2 μM as the tetramer) was loaded onto the GAN-immobilized chip for 120 s followed by washing with running buffer for 90 s and then MCM (2 μM as the hexamer) was loaded onto the GINS-bound GAN-chip for 120 s (upper sensorgram). The injections of the analytes are indicated by the arrows on the sensorgrams.

Analyses of GAN, GINS and MCM in *T. kodakarensis* cells

The intracellular amounts of GINS and GAN in exponentially growing *T. kodakarensis* cells were measured by western blot analyses, using anti-GAN and anti-Gins51 antisera, based on a comparison of the band intensities from the cell extract and from serial dilutions of each purified protein (Figure 2A). The calculated amounts of the GAN and Gins51 proteins were 300–400 molecules/cell (as the monomer) and 200–300 molecules/cell (as the dimer), respectively. The concentration of MCM was also similar (200–300 molecules/cell, as the hexamer), as reported previously (20). The comparable number of each molecule in the cells may suggest that MCM, GINS and GAN mostly work together. Their intracellular concentrations should be about 0.5 μM in a *T. kodakarensis* cell, calculated from a spherical cell with a 1.5 μm diameter. To investigate whether the GAN, GINS and MCM proteins form a complex in the *T. kodakarensis* cells, an immunoprecipitation experiment was performed. The immunocomplexes were captured with anti-GAN, anti-Gins51, anti-Gins23 or anti-MCM antibodies from the whole extracts. The immunocomplexes were subjected to SDS-PAGE, followed by western blot analyses using each antibody. As shown in Figure 2B, GAN, GINS and MCM were co-precipitated with either anti-GAN, anti-Gins51, anti-Gins23 or anti-MCM antibodies. These results suggest that the GAN, GINS and MCM proteins are co-localized in the same complex in *T. kodakarensis* cells, although final confirmation of its occurrence must await detection of the GAN·GINS·MCM complex in *T. kodakarensis* cell extracts.

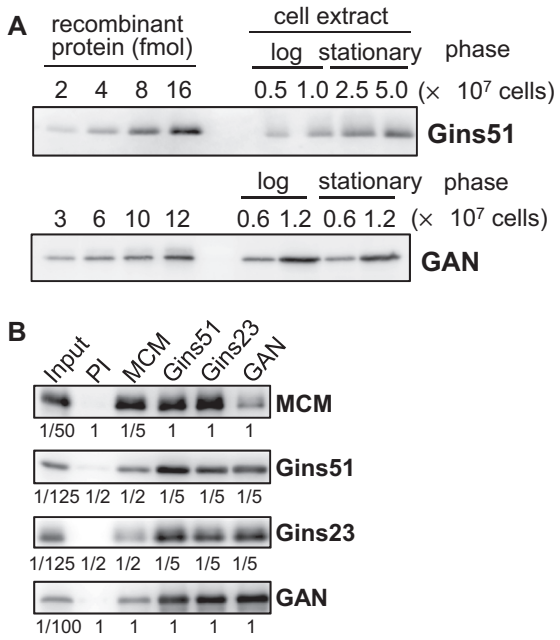

Figure 2. Formation of the GAN·MCM·GINS complex in *T. kodakarensis* cells. (**A**) Estimation of the intracellular concentrations of GINS and GAN in *T. kodakarensis* cells. The loading amounts and detection conditions were different, depending on the activities of the antibodies. (**B**) Immunoprecipitation of GAN, GINS and MCM from the *T. kodakarensis* cell extract. The immunocomplexes were captured individually with each antiserum from the whole cell extract (as shown at the top) and were subjected to SDS-10% PAGE (for MCM) or SDS-12.5% PAGE (for GAN, Gins51 and Gins23), followed by western blot analyses using these antisera (shown on the right side). The whole cell extracts without immunoprecipitation (Input) and those precipitated after a treatment with preimmune serum (PI) were also loaded as positive and negative controls, respectively. The relative loading amounts are indicated at the bottom of the panels.

Effects of GINS and GAN on the helicase and ATPase activities of MCM

The ternary complex of GAN·GINS·MCM was detected *in vitro*. The question to be answered is whether GAN is actually involved in the replicative helicase complex in *T. kodakarensis* and if so, what is the function of GAN in fork progression? GINS clearly stimulates the ATPase and helicase activities of MCM *in vitro*, as we showed previously (20). We examined how the GAN·GINS complex affects the ATPase and helicase activities of MCM. As shown in Figure 3A, GAN did not stimulate the helicase activity of MCM by itself. Rather GAN slightly suppressed the helicase activity of MCM (lanes 4, 7–10). A competition for DNA binding may have occurred between MCM and GAN under this assay condition. The GAN·GINS complex clearly stimulated the activity of MCM, although they were slightly suppressed as compared with the case of GINS alone (lanes 4, 11–15). To investigate in more detail whether GAN affects the affinity between GINS and MCM in the presence of DNA, ATPase assays were performed with increasing amounts of GAN and GINS (Figure 3B). MCM showed a dsDNA-dependent ATPase activity, which was not clearly stimulated by GINS as reported previously (20). GAN did not stimulate the activity by itself and furthermore, GAN did not stimulate the dsDNA-dependent ATPase activity of the MCM·GINS complex. On the other hand, the ssDNA-dependent ATPase activity was clearly stimulated by GINS as reported previously (20), but addition of GAN did not affect this stimulation. These results suggest that GAN does not affect the affinity of MCM·GINS interaction in the presence of DNA. The basal ATPase activity of MCM was temperature dependent. However, effects of GINS and GAN·GINS on MCM at 60°C were not different from those at 70°C as described above (Supplementary Figure S2).

In the cells, RPA should work to bind the single-stranded region of DNA. Therefore, we added the recombinant *T. kodakarensis* RPA complex (Supplementary Figure S3) in the helicase assays using the same synthetic dsDNA with splayed arms. As shown in Figure 3C, RPA bound the ssDNA produced by MCM helicase (lane 4) and the amount of the RPA-bound DNA was increased by addition of either GINS (lanes 5–7) or GAN·GINS (lanes 8–10). These RPA-bound DNAs were quantified and plotted in Figure 3D, showing that the stimulation of the MCM helicase activity was not different between GINS and GAN·GINS. This experiment also supported that GAN did not stimulate the helicase activity. This experiment including RPA suggested, at least, that GAN·GINS-stimulated MCM helicase works without any inhibition *in vitro* in the presence of RPA. In terms of the function of RPA, a recent report showed that human Cdc45 positively loads RPA onto nascent ssDNA (48). We investigated here if a sufficient amount of RPA affects the unwinding efficiency of MCM helicase in the presence of GINS and GAN. More detailed biochemical analyses, including the loading of RPA by GAN, should be interesting in this archaeal system.

These data presented here indicate that GAN does not synergistically stimulate the helicase and ATPase activities with GINS *in vitro*, in contrast to the clear stimulation of the GAN nuclease by GINS (29,35), but at least GAN does not interfere with GINS in stimulating MCM activity.

Exonuclease activity of GAN

GAN is a ssDNA specific 5′–3′ exonuclease that generates mononucleotide products, in a manner similar to bacterial RecJ, as described previously (29,49). We investigated whether the nuclease activity of GAN is related to replication fork progression. The alanine substitution of the metal-binding residue in motif I (GAN-D36A), predicted from the bacterial RecJ, was prepared (Supplementary Figure S4A) and used for the nuclease assay. This mutation almost completely inactivated GAN (Supplementary Figure S4B, lane 6). The loss of the exonuclease activity in GAN-D36A is consistent with the results of equivalent mutations in bacterial RecJs and archaeal RecJ-like proteins (50–52). For the *T. kodakarensis* GAN, the D34A mutant also lost the nuclease activity, as previously reported (29). The effect of the GAN-D36A mutant on the MCM helicase activity was examined in parallel with the WT GAN and we obtained the same results with GAN-D36A as that with the WT GAN (Supplementary Figure S4C and Figure 3A).

We characterized the 5′–3′ exonuclease activity of GAN in more detail. As shown in Supplementary Figure S5A, GAN exhibited 5′–3′ exonuclease activity and the proces-

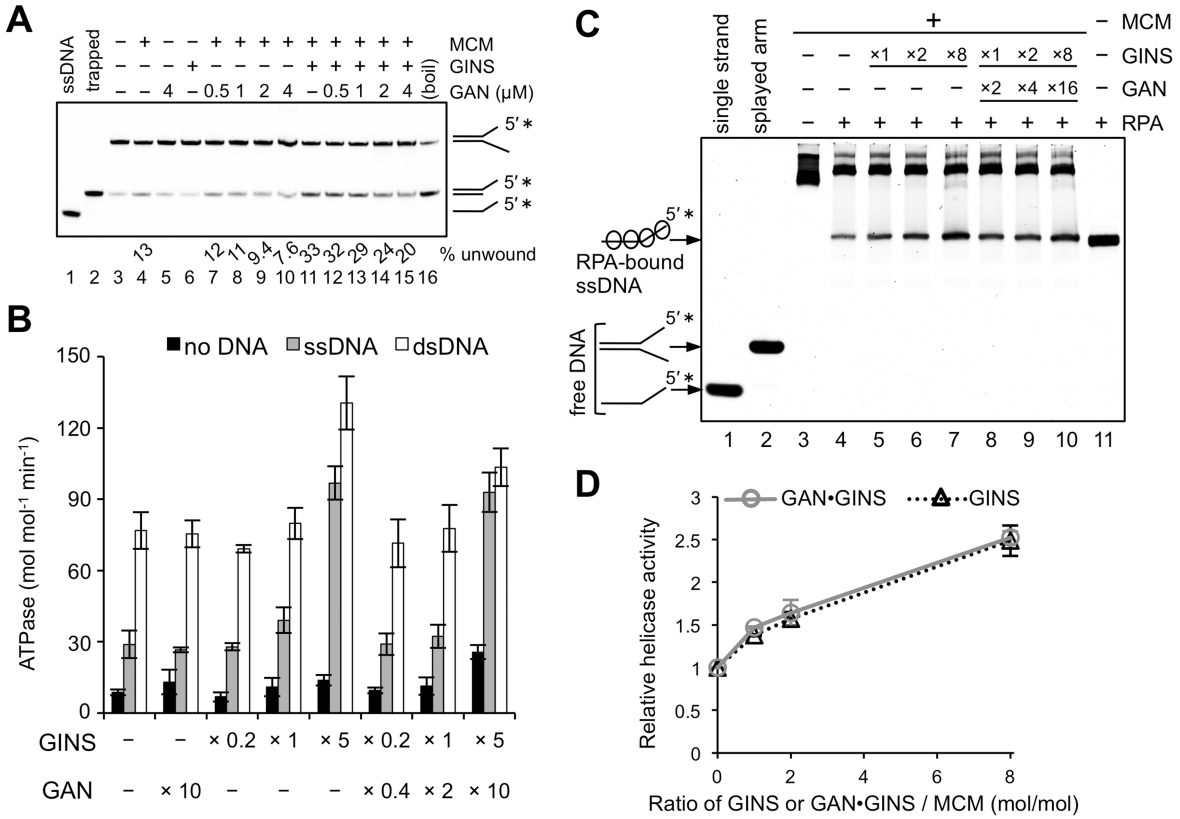

Figure 3. Effects of GINS and GAN on the helicase and ATPase activities of MCM. (**A**) The helicase activity of MCM in the presence of the GAN·GINS complex. The 5′-Cy5-labeled (*) splayed arm DNA substrate (50 nM) was incubated with MCM, GINS and GAN. The helicase activity is expressed at the bottom of the panel, as the relative amount of unwound DNA (%). Single-stranded and trapped DNAs were loaded in parallel as controls for the unwinding reaction (lanes 1 and 2, respectively). The same results were obtained thrice and a representative gel image is shown. (**B**) The ATPase activity of MCM in the presence of the GAN·GINS complex with various ratios (0.2-, 1- and 5-folds for GINS and 0.4-, 2- and 10-folds for GAN) to the constant amount of MCM. The ATPase activity is expressed as the amount of PI released by a constant amount of the MCM protein (as the hexamer) in the absence or presence of circular ssDNA or dsDNA. The SEM was calculated from three independent experiments. (**C**) Effect of replication protein A (RPA) on the helicase assay using MCM, GINS, GAN·GINS and the 5′-Cy5-labeled (*) splayed arm DNA without trap DNA. The reaction mixtures were loaded on the gel without denaturing. The DNA structures corresponding to each band were indicated at the left side. The RPA-bound ssDNA is shown in lane 11 as a control. (**D**) Quantification of unwinding activity with RPA. The RPA-bound ssDNAs in panel C were quantified and plotted. The SEM was calculated from three independent experiments.

sive reaction obviously paused at the phosphorothioate sites (Supplementary Figure S5B). Furthermore, the reaction stopped in front of the dsDNA regions from a 5′- overhang DNA substrate (Supplementary Figure S5C, lanes 8 and 9). We next examined the nuclease activity of GAN in the presence or absence of GINS and MCM. The GAN·GINS complex, obtained by mixing these proteins in an equimolar ratio, showed 1.5-fold higher nuclease activity than that in the absence of GINS (Figure 4). The cleavage efficiencies of GAN were not affected by increasing amounts of MCM in the reaction mixtures, both in the presence and absence of GINS (Figure 4). These results indicated that MCM does not have any effect on the nuclease activity of GAN by alone and also of GAN complexed with GINS.

The effect of a divalent ion on the nuclease activities of GAN and the GAN·GINS complex

GAN showed Mn^{2+}-dependent exonuclease activity and had limited activity with Mg^{2+} (Figure 5A, compare lane 2 with 10 or lane 12 with 20), as observed previously (29). GINS and Gins51 stimulate the exonuclease activity of GAN in the presence of $MnCl_2$ (29,35). The nuclease activity of GAN was not stimulated by GINS in reaction conditions containing Mg^{2+} alone (Figure 5A, compare lane 2 with lanes 4–6). However, the nuclease was stimulated by GINS in the presence of 1 mM Mn^{2+} and 2 mM Mg^{2+} (Figure 5A, compare lanes 17, 18 and 19). The nuclease activity of GAN·GINS in the presence of 1 mM Mn^{2+} and 2 mM Mg^{2+} was similar to that with 1 mM Mn^{2+} alone (Figure 5A, compare lane 16 with lane 19). Together, these results show that the Mn^{2+} ion is preferable for the exonuclease activity of GAN.

Measurement of metal concentrations in *T. kodakarensis* cells

To address the question whether GAN works as an exonuclease in *T. kodakarensis* cells, we quantified the intracellular concentrations of Mg and Mn. The measurements of metal concentrations were performed using whole cells and cell extracts as the solid and liquid samples, respectively. As

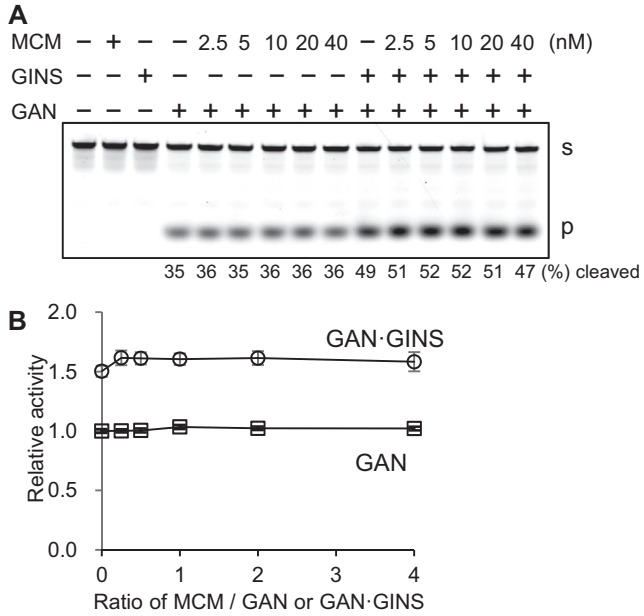

Figure 4. The effect of MCM on the nuclease activities of GAN and the GAN·GINS complex. (**A**) The reaction mixtures (20 μl), containing 25 mM Bis–Tris, pH 7.0, 125 μg/ml BSA, 1 mM DTT, 2 mM $MnCl_2$, 2 μM 3′-FITC-labeled DNA (dA30-FITC), 10 nM GAN, 10 nM GINS (as the tetramer) and MCM (2.5, 5, 10, 20 and 40 nM as the hexamer), were preincubated without $MnCl_2$ for 3 min at 60°C and then incubated with $MnCl_2$ for 2 min at 60°C. The reaction was terminated by adding 5 μl stop solution A and immediately transferred onto ice. Products were subjected to 20% native PAGE. The band assignments are indicated on the side of the panel: s, substrates; p, cleaved products. (**B**) The quantified nuclease activities of GAN (open squares) and the GAN·GINS complex (open circles) in the presence of various concentrations of MCM in panel A were plotted. The SEM was calculated from three independent experiments.

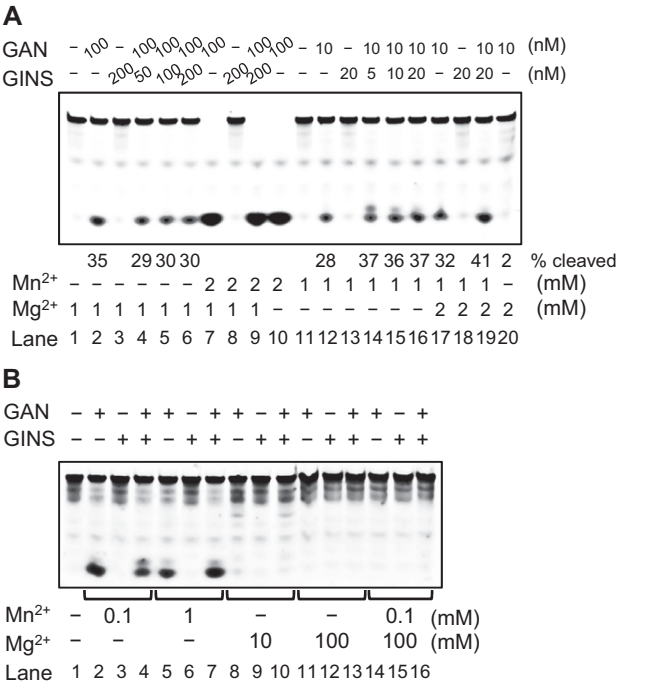

Figure 5. The effect of divalent ions on the nuclease activities of GAN and the GAN·GINS complex. The reaction products of 3′-FITC-labeled ssDNA (1 μM) were separated by native 20% PAGE in TBE. (**A**) The reaction mixtures were incubated without GAN for 3 min at 60°C and then GAN was added and the reactions were incubated at 60°C for 10 min (lanes 1–10) or 2 min (lanes 11–20). In lanes 7–9 and 17–19, both $MnCl_2$ and $MgCl_2$ were included in the reaction solutions. The concentrations of the proteins and metals are shown at the top and the bottom, respectively, of the panel. (**B**) The reaction mixtures were incubated without GAN for 3 min at 60°C and then reacted with 10 nM GAN, with or without 20 nM GINS, at 60°C for 10 min. In lanes 14–16, both 0.1 mM $MnCl_2$ and 100 mM $MgCl_2$ were included in the reaction solutions. The metal concentrations in each reaction are shown at the bottom of the panel.

shown in Table 1, nearly equal amounts of metal per cell were calculated from the solid and liquid samples. The resultant concentrations of Mg and Mn were about 120 and 0.12 mM, respectively. The Mg to Mn ratio in the cell is about 1000 to 1. The GAN nuclease activity in the presence of 0.1 mM Mn^{2+} was actually suppressed by 100 mM Mg^{2+} *in vitro* (Figure 5B, compare lanes 2, 4 and 14, 16). These results suggest that GAN does not function as a nuclease, regardless of whether it is complexed with GINS in the *T. kodakarensis* cells.

Growth properties of the *T. kodakarensis* Δ*gan* strain

If the function of the CMG complex is conserved in Eukarya and Archaea, then GAN should be essential for the viability of *T. kodakarensis*. To test whether this is the case, gene disruption of the *gan* gene was carried out. We employed the pop-in/pop-out strategy that consists of a single crossover integration of a disruption plasmid into the chromosome followed by a second pop-out recombination that removes the *pyrF* marker gene (53). According to the procedure, the *pyrF*-strains obtained after the second recombination should consist of two types of cells, those that returned to the host cell genotype and gene disruptants. When the gene targeted for disruption is not essential and the transformants are not grown in liquid culture prior to selection, the ratio of the two types should be, in principle, 1:1. We successfully isolated a strain with the deletion of the *gan* gene. PCR amplification from the *gan* region in the Δ*gan* mutant strain produced a DNA product with the predicted size, corresponding to the lengths of the 5′ and 3′ flanking regions of the targeted loci without the GAN-coding regions (Supplementary Figure S6). From a total of 36 colonies examined, 20 colonies harbored the *gan* gene deletion. Therefore, GAN was not essential for the viability of *T. kodakarensis* at least under the conditions employed for selection (growth in ASW-YT-S^0 medium at 85°C) suggesting that the GAN protein is not an essential component of the replisome. However, we found that the Δ*gan* mutant showed a clear growth retardation at around 0.1 OD_{660} as compared with the parental cells, under the optimal growth conditions although no difference from 0.01 to 0.1 OD_{660} was detected. Because it is difficult to measure the low density at the initial stage with the sulfur powder, we used pyruvate-based medium to compare the growth curve more precisely and found the characteristic growth retardation of the Δ*gan* mutant. Furthermore, when the cells were cultivated at 93°C, the Δ*gan* cells showed a more obvious growth defect (Figure 6A). These growth defects were reproducibly observed more than three-times each for three

Table 1. Intracellular concentrations of magnesium and manganese ions in *T. kodakarensis*

Element	Measured				Calculated (per cell)					Estimated
	Solid sample (mg/kg)		Liquid sample (mg/l)		Solid sample ($\times 10^{-15}$ mol/cell)		Liquid sample ($\times 10^{-15}$ mol/cell)		Average ($\times 10^{-15}$ mol/cell)	Intracellular conc.
	ICP-MS	ICP-AES	ICP-MS	ICP-AES	ICP-MS	ICP-AES	ICP-MS	ICP-AES		
Mg	370	390	53	59	0.23	0.24	0.17	0.18	0.21	120 mM
Mn	0.82	N.D.	0.14	N.D.	0.00023	N.D.	0.00019	N.D.	0.00021	0.12 mM

N.D., not determined.

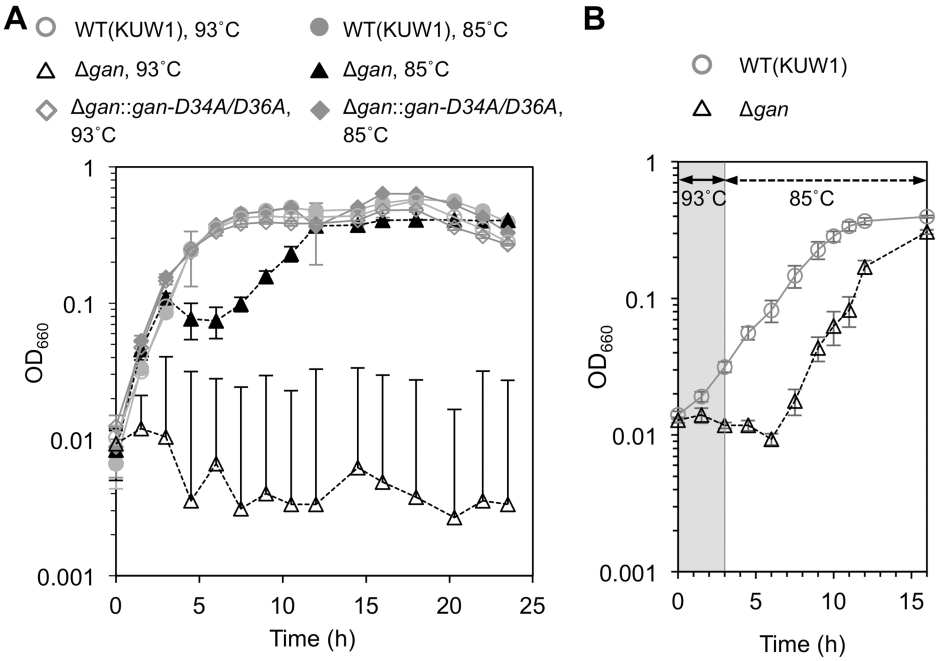

Figure 6. The disruption of the *gan* gene led to obvious growth retardation and a temperature-sensitive phenotype. (**A**) Growth properties of the *T. kodakarensis* KUW1, Δ*gan* and Δ*gan::gan-D34A/D36A* strains in ASW-YT-Pr at 85 and 93°C. Symbols are indicated on the top of the panels. OD_{660}, turbidity at 660 nm. Each strain was examined at least thrice and error bars represent SEM. Only the plus error bars are indicated for the Δ*gan* strain at 93°C. (**B**) The cells were cultured for 3 h at 93°C, then the temperature was shifted to 85°C to continue the cultivation. The gray background indicates the period at 93°C.

independently isolated strains. The growth defect at high temperature of the Δ*gan* mutant was reversibly recovered by the temperature-shift back to 85°C after culturing for 3 h at 93°C. It took 8 h to reach 0.1 OD_{660} (Figure 6B). When the cultures were kept at 93°C for 6 and 12 h, they reached 0.1 OD_{660} after 24 and 36 h, respectively, since the culture restarted at 85°C. These results may suggest that the temperature-sensitive phenotype of the Δ*gan* mutant is derived from insufficient progression of the replication fork and that the number of cells that survived the high temperature decreased depending on the length of the incubation period at 93°C. We performed a targeted insertion of the nuclease-defect *gan* gene (*gan-D34A/D36A*) into the Δ*gan* strain. The resultant strain, Δ*gan*::*gan-D34A/D36A*, did not show any growth defect, indicating that the nuclease activity of GAN is not required for GAN to function during normal cell growth.

Growth defects of the Δ*gan* strain are caused by the loss of GAN

The *gan* gene is predicted to exist in an operon with two ribosomal proteins, universal S15 and archaeo-eukaryotic S3, and the Pcc1 subunit of the KEOPS complex, which is involved in an essential tRNA modification and possibly other functions related to translation (28), in the *T. kodakarensis* genome (Figure 7A). Although our complementation experiments indicated otherwise, we nevertheless examined whether the growth defect of the Δ*gan* strain was attributed to the instability of the expression of the neighboring genes in the predicted operon. The *gan* gene overlaps with *pcc1* for 23 nt. The deletion of the *gan* gene left the *pcc1* gene intact. The Δ*gan* genome was confirmed *via* direct sequencing, to verify that an unexpected alteration did not occur in the flanking region. To investigate the expression level of each gene in the predicted operon, we first analyzed the length of the mRNA including the *gan* gene. The DNA fragments with the predicted sizes were successfully amplified from the cDNAs of the KUW1 and the Δ*gan* cells by the primers, which were designed based on the operon structure (Figure 7B), indicating that the *gan* gene is involved in an operon and it is transcribed together with *rps15*, *pcc1* and *rps3*. The PCR products from the Δ*gan* cDNA indicated that this operon is transcribed in the *T. kodakarensis* cells, even in the absence of the *gan* gene. We then quantified

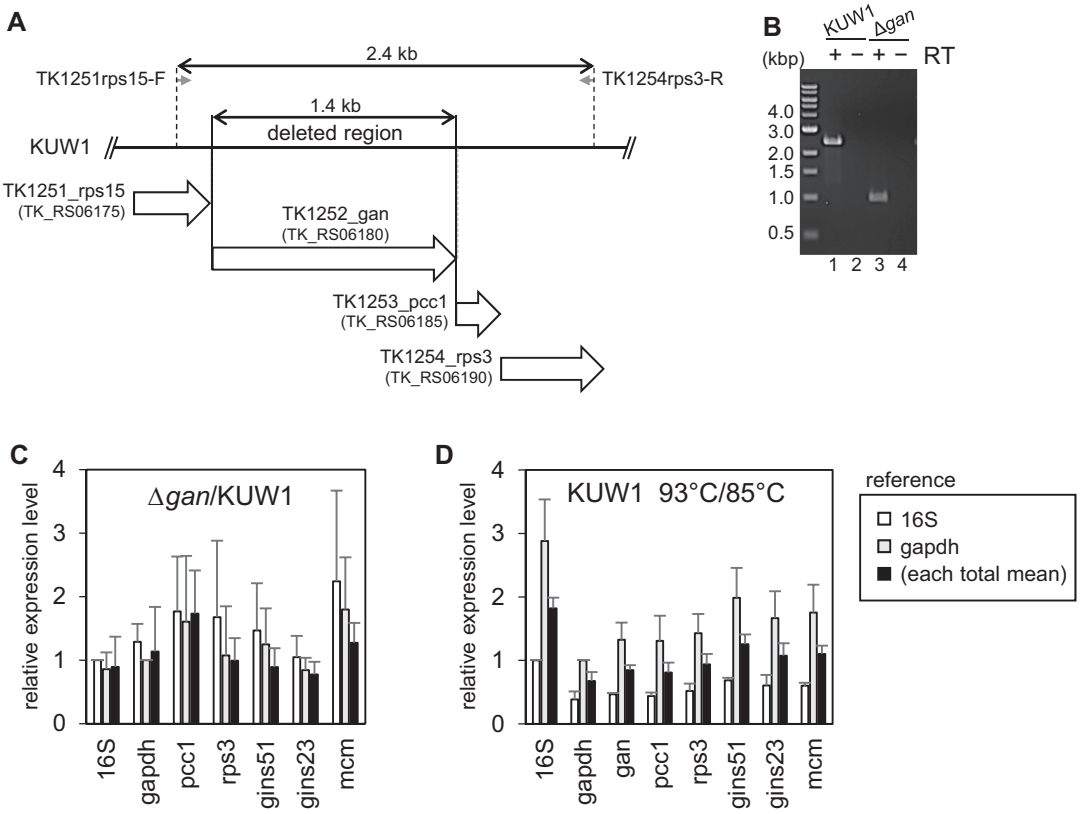

Figure 7. Expression levels of the genes in *T. kodakarensis.* (**A**) Schematic map of the gene organization at the *gan* locus in the *T. kodakarensis* genome. The expected PCR product from the cDNA, which is reverse-transcribed from the mRNA from the predicted operon of *rps15-gan-pcc1-rps3* in KUW1, is 2409 bp, by using the TK1251rps15-F/TK1254rps3-R primer set. (**B**) Determination of the operon structure. The DNA fragments with the predicted sizes were amplified from the cDNA samples (after RT, lane '+') but not from the mRNAs (before RT, lane '−'). (**C**) Relative amounts of mRNA for the *pcc1, rps3, gins51*, *gins23* and *mcm* genes were compared between KUW1 and Δ*gan,* and are shown as the ratio of Δ*gan*/KUW1. The mRNA levels were normalized using multiple reference genes, the 16S rRNA (white bars), *gapdh* (gray bars) and each total mean level (black bars). Data shown in the graph are averages of three independent experiments with the SEM. (**D**) Relative mRNA levels of the 16S rRNA, *gapdh, gan, pcc1, rps3, gins51*, *gins23* and *mcm* genes in KUW1 were compared between 85 and 93°C, and are shown as the ratio of 93°C/85°C. The mRNA levels were normalized using multiple reference genes, the 16S rRNA (white bars), *gapdh* (gray bars) and each total mean level (black bars). Data shown in the graph are averages of three independent experiments with the SEM.

the mRNAs of the *pcc1* and *rps3* genes, located downstream of the *gan* gene. The relative abundances of these mRNAs were the same between KUW1 and Δ*gan*, indicating that the deletion of the *gan* gene does not affect the transcription efficiency of the downstream genes. We also confirmed that the expression levels of the *gins51*, *gins23* and *mcm* genes in the cells were the same in the presence and absence of the *gan* gene (Figure 7C).

To examine the temperature-sensitive phenotype of the Δ*gan* mutant, we measured the relative abundances of the *gan*, *pcc1*, *rps3*, *gins51*, *gins23* and *mcm* mRNAs in *T. kodakarensis* KUW1, grown at 85 and 93°C. None of the genes showed any significant differences in expression between 85 and 93°C (Figure 7D). The amount of the GAN protein in the cells was confirmed to be the same among the KUW1, Δ*gan* and Δ*gan*::*gan-D34A/D36A* strains (Supplementary Figure S7). These results indicate that the temperature-sensitivity of the Δ*gan* mutant was not derived from the inactivation of the nuclease, but from the absence of the GAN protein in the cells.

UV sensitivity of the *T. kodakarensis* Δ*gan* strain

To further examine whether GAN is involved in some DNA repair system in *T. kodakarensis,* we compared the DNA damage sensitivity of the Δ*gan* mutant to that of the parental cells. We monitored how the knockout of the *gan* gene impacted the cell viability after DNA-damaging treatments, by a drop dilution assay. Although the Δ*gan* cells formed smaller colonies than those of the parental KUW1 cells under the same conditions, the Δ*gan* cells exhibited the same viability as the parental KUW1 strain under the conditions without any DNA-damaging treatment (Figure 8A). However, the Δ*gan* cells could not form colonies upon cultivation at 93°C for 24 h (Figure 8B). This temperature sensitive phenotype of the Δ*gan* mutant was consistent with the results from the liquid culture, as shown in Figure 6. The bacterial *recj* mutant also showed a UV-sensitive phenotype (54–56). Therefore, we examined the UV-sensitivity of the *T. kodakarensis* Δ*gan* mutant. Each strain was serially diluted and spotted on a plate, and was irradiated by UV-C (254 nm). However, differences in the phenotypes were not observed between the KUW1 and the Δ*gan* mutant strains (Figure 8). These experimental data suggest that GAN is

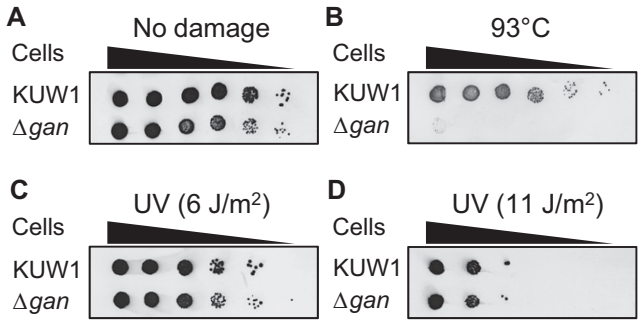

Figure 8. Viability of Δ*gan* mutant *T. kodakarensis*. Drop dilution assays for the sensitivities of KUW1 and Δ*gan* cells to 93°C and UV-C. The serially-diluted *T. kodakarensis* cells (6×10^5, 6×10^4, 6×10^3, 6×10^2, 6×10^1 and 6×10^0 cells from left to right) were spotted on the plates before the treatment, as described in the 'Materials and Methods' section. The plates were then incubated anaerobically at 85°C (**A**, **C** and **D**) and 93°C (**B**).

not involved in the repair pathway for UV-damaged DNA, although such a repair pathway has not yet been identified in *T. kodakarensis* cells.

DISCUSSION

The structures and functions of replicative helicase complexes are popular topics in research on the mechanism of DNA replication. Many reports about the structure of the eukaryotic CMG complex, as a replicative helicase, have been published (10–17). In this study, we presented the CMG-like complex, which is actually GAN·MCM·GINS, in the hyperthermophilic euryarchaeon, *T. kodakarensis*. A very stable GAN·GINS complex was detected, using the purified proteins. MCM bound to GINS, but not to GAN and therefore, the formation of the ternary complex is made possible by the interactions of GAN–GINS and GINS–MCM. This mode of the CMG-like complex formation is different from that in Eukarya. Cdc45 is apparently recruited to the MCM ring, followed by GINS and Cdc45 interacts with both GINS and MCM. The crystal structure of Cdc45 was docked with the EM map of the CMG complex. Cdc45 wedges its CID between the adjacent A-subdomains of Mcm5 and Mcm2, to stabilize the N-terminal ring of MCM2–7. This association is required for the helicase activity and the replisome assembly. Furthermore, a molecular break model has been proposed, in which Cdc45 controls the progression of CMG helicase and slows it down when the replication fork is stalled, by the disassembly of the CMG complex to prevent excessive generation of the single-stranded region, based on the DNA binding ability of Cdc45 (57,58). In contrast, the archaeal GAN does not interact with MCM. Actually, we found that the helicase activity of MCM is not affected by the presence of GINS and GAN·GINS *in vitro*, in this study. Recent reports about the archaeal CMG-like complexes from *T. acidophilum* (32) and *Sulfolobus* species *(S. acidocaldarius* and *S. islandicus)* (30) have been published. These reports also showed the CMG-like complex formation, but the RecJ/Cdc45 proteins did not interact with MCM directly. These reports also support the finding that the assembly mode of the archaeal GAN·MCM·GINS seems to be quite different from that of the eukaryotic CMG complex. The EM analysis of the archaeal GAN·MCM·GINS, which is currently underway in our group, will provide critical information about the conservation and divergence of the structural role of GAN in the CMG-like complex. It is noteworthy that the *Sulfolobus* GINS does not stimulate the MCM helicase, but it is clearly stimulated in the presence of both GINS and the Cdc45/RecJ protein *in vitro* (30). Therefore, the structures and functions of the CMG-like complex are divergent even in the archaeal domain.

A second important issue is the nuclease function of GAN in the cells. In contrast to the absence of nuclease activity in the eukaryotic Cdc45, the archaeal GAN has a bacterial RecJ-like 5′–3′ exonuclease activity, which is stimulated by GINS *in vitro* (29,35 and this study). The authors of the report describing the GINS-stimulated nuclease proposed the hypothesis that GAN works to remove the primers in the lagging strand synthesis by a similar mode to the bacterial PolI protein (29). The genetic analyses of GAN, Fen1 and RNase HII showed that the double mutant of GAN and RNase HII also could not be isolated (37). The authors discussed that the reason why the Fen1 and RNase HII double mutant grew well is that GAN supported the Okazaki fragment maturation by itself, in the absence of Fen1 and RNase HII. They proposed from their genetic works that the exonuclease activity of GAN functions for the removal of primers during Okazaki fragment maturation. It is an interesting hypothesis, but It has not been elucidated yet whether GAN exerts its nuclease activity on DNA or RNA in the *T. kodakarensis* cells.

We carefully analyzed the nuclease activity of GAN *in vitro* in this study. The nuclease activity is clearly dependent on Mn^{2+}, rather than Mg^{2+}, as shown in this study and the previous report (29) but the Mn^{2+}-dependent nuclease activity is strictly suppressed by excess amounts of Mg^{2+}. Therefore, we quantified the intracellular concentrations of Mg and Mn in *T. kodakarensis* and found that they were about 120 and 0.1 mM, respectively. The ratio of Mg to Mn in the cell is 1000 to 1. We then confirmed that the nuclease activity of GAN is not observed under such conditions *in vitro*. These results support the proposal that GAN does not work as a nuclease in the CMG-like complex in *T. kodakarensis* cells. The Cdc45/RecJ-like protein in *Sulfolobus* strains formed a CMG-like complex and stimulated the MCM helicase, as described above (30) but it lacks the nuclease domain (31). This fact also supports the idea that the Cdc45/RecJ-like protein in Archaea may only have a structural role for the active helicase and the nuclease activity is not required for this task, as shown in Eukarya. RecJ in *D. radiodurans* reportedly employs Mn^{2+} for catalysis and its 5′–3′ exonuclease activity is detectable under conditions with 0.1 mM Mn^{2+} and 10 mM Mg^{2+}, and even with 100 mM Mg^{2+} (59), in contrast to *T. kodakarensis* GAN. The RecJ in *D. radiodurans* is probably a nuclease, as observed in Bacteria. The RecJ homolog from *Methanocaldococcus jannaschii,* a methanogenic archaeon, can partially complement the *recJ* mutant phenotype (UV sensitivity) of *E. coli* (60). Therefore, like bacterial RecJs, the RecJ homolog in *M. jannaschii* should work in the repair pathway for UV-damaged DNA. However, the Δ*gan* mutant of *T. kodakarensis* did not show any UV sensitivity in our analysis.

Our analyses of the Δ*gan* mutant revealed a clear growth retardation as compared with the parental KUW1 cells under the optimal growth conditions, and the Δ*gan* mutant did not grow at 93°C. Furthermore, the temperature-sensitive and growth retardation phenotypes were complemented by returning the nuclease-defect *gan* gene back to the genome. These genetic analyses also support the proposal that the nuclease activity is not related to the growth defect of the Δ*gan* mutant. Based on these phenotypes, we speculate that the replicative helicase complex became less stable without GAN, resulting in the deceleration of replication fork progression, as compared with the WT GAN·GINS·MCM complex. Furthermore, the helicase complex may lose the activity that facilitates the functional progress of the replication fork at 93°C. Our helicase assay at 65°C, using short oligonucleotides, did not reveal any differences in the presence and absence of GAN. To verify our hypothesis, we are now constructing an assay system for the helicase activity using a long DNA strand, to compare the activities of the helicase complex with and without GAN at various temperatures *in vitro*.

Taking together all of our experimental data presented here, the nuclease activity of GAN does not seem to be relevant in *T. kodakarensis* cells, even though the important residues of the nuclease domain are strictly conserved and the 5′–3′ exonuclease activity was actually detected *in vitro.* Notably, the nuclease activity of GAN is not necessary in *T. kodakarensis* cells for the normal growth. We cannot rule out the possibility that other proteins interact with GAN and somehow incorporate Mn into its active site. This would trigger the nuclease activity of GAN, which may be involved in a currently unidentified function. Further studies are required to understand the physiological reason of the growth defects by GAN deletion and to elucidate the exact function of GAN in *T. kodakarensis* cells.

SUPPLEMENTARY DATA

Supplementary data are available at NAR Online.

FUNDING

This work was supported by Ministry of Education, Culture, Sports, Science and Technology of Japan [JP21113005, JP23310152, JP26242075 to Y. I.]; Grant-in-Aid for Japan Society for the Promotion of Science (JSPS) Fellows [JP16J02633 to M.N.]. Funding for open access charge was supported by JSPS [JP16J02633].
Conflict of interest statement. None declared.

REFERENCES

1. Masai,H., Matsumoto,S., You,Z., Yoshizawa-Sugata,N. and Oda,M. (2010) Eukaryotic chromosome DNA replication: where, when, and how? *Annu. Rev. Biochem.*, **79**, 89–130.
2. Ishino,Y. and Ishino,S. (2012) Rapid progress of DNA replication studies in Archaea, the third domain of life. *Sci. China Life Sci.*, **55**, 386–403.
3. Mott,M.L. and Berger,J.M. (2007) DNA replication initiation: mechanisms and regulation in bacteria. *Nat. Rev. Microbiol.*, **5**, 343–354.
4. Aparicio,O.M., Weinstein,D.M. and Bell,S.P. (1997) Components and dynamics of DNA replication complexes in *S. cerevisiae*: redistribution of MCM proteins and Cdc45p during S phase. *Cell*, **91**, 59–69.
5. Takayama,Y., Kamimura,Y., Okawa,M., Muramatsu,S., Sugino,A. and Araki,H. (2003) GINS, a novel multiprotein complex required for chromosomal DNA replication in budding yeast. *Genes Dev.*, **17**, 1153–1165.
6. Kubota,Y., Takase,Y., Komori,Y., Hashimoto,Y., Arata,T., Kamimura,Y., Araki,H. and Takisawa,H. (2003) A novel ring-like complex of *Xenopus* proteins essential for the initiation of DNA replication. *Genes Dev.*, **17**, 1141–1152.
7. Gambus,A., Jones,R.C., Sanchez-Diaz,A., Kanemaki,M., van Deursen,F., Edmondson,R.D. and Labib,K. (2006) GINS maintains association of Cdc45 with MCM in replisome progression complexes at eukaryotic DNA replication forks. *Nat. Cell Biol.*, **8**, 358–366.
8. Moyer,S.E., Lewis,P.W. and Botchan,M.R. (2006) Isolation of the Cdc45/Mcm2-7/GINS (CMG) complex, a candidate for the eukaryotic DNA replication fork helicase. *Proc. Natl. Acad. Sci. U.S.A.*, **103**, 10236–10241.
9. Pacek,M., Tutter,A.V., Kubota,Y., Takisawa,H. and Walter,J.C. (2006) Localization of MCM2-7, Cdc45, and GINS to the site of DNA unwinding during eukaryotic DNA replication. *Mol. Cell*, **21**, 581–587.
10. Ilves,I., Petojevic,T., Pesavento,J.J. and Botchan,M.R. (2010) Activation of the MCM2-7 helicase by association with Cdc45 and GINS proteins. *Mol. Cell*, **37**, 247–258.
11. Costa,A., Ilves,I., Tamberg,N., Petojevic,T., Nogales,E., Botchan,M.R. and Berger,J.M. (2011) The structural basis for MCM2-7 helicase activation by GINS and Cdc45. *Nat. Struct. Mol. Biol.*, **18**, 471–477.
12. Costa,A., Renault,L., Swuec,P., Petojevic,T., Pesavento,J.J., Ilves,I., MacLellan-Gibson,K., Fleck,R.A., Botchan,M.R. and Berger,J.M. (2014) DNA binding polarity, dimerization, and ATPase ring remodeling in the CMG helicase of the eukaryotic replisome. *Elife*, **3**, e03273.
13. Sun,J., Shi,Y., Georgescu,R.E., Yuan,Z., Chait,B.T., Li,H. and O'Donnell,M.E. (2015) The architecture of a eukaryotic replisome. *Nat. Struct. Mol. Biol.*, **22**, 976–982.
14. Li,N., Zhai,Y., Zhang,Y., Li,W., Yang,M., Lei,J., Tye,BK. and Gao,N. (2015) Structure of the eukaryotic MCM complex at 3.8 Å. *Nature*, **524**, 186–191.
15. Abid Ali,F., Renault,L., Gannon,J., Gahlon,H.L., Kotecha,A., Zhou,J.C., Rueda,D. and Costa,A. (2016) Cryo-EM structures of the eukaryotic replicative helicase bound to a translocation substrate. *Nat. Commun.*, **7**, 10708.
16. Yuan,Z., Bai,L., Sun,J., Georgescu,R., Liu,J., O'Donnell,M.E. and Li,H. (2016) Structure of the eukaryotic replicative CMG helicase suggests a pumpjack motion for translocation. *Nat. Struct. Mol. Biol.*, **23**, 217–224.
17. Georgescu,R., Yuan,Z., Bai,L., de Luna Almeida Santos,R., Sun,J., Zhang,D., Yurieva,O., Li,H. and O'Donnell,M.E. (2017) Structure of eukaryotic CMG helicase at a replication fork and implications to replisome architecture and origin initiation. *Proc. Natl. Acad. Sci. U.S.A.*, **114**, E697–E706.
18. Sakakibara,N., Kelman,L.M. and Kelman,Z. (2009) Unwinding the structure and function of the archaeal MCM helicase. *Mol. Microbiol.*, **72**, 286–296.
19. Yoshimochi,T., Fujikane,R., Kawanami,M., Matsunaga,F. and Ishino,Y. (2008) The GINS complex from *Pyrococcus furiosus* stimulates the MCM helicase activity. *J. Biol. Chem.*, **283**, 1601–1609.
20. Ishino,S., Fujino,S., Tomita,H., Ogino,H., Takao,K., Daiyasu,H., Kanai,T., Atomi,H. and Ishino,Y. (2011) Biochemical and genetical analyses of the three *mcm* genes from the hyperthermophilic archaeon. *Genes Cells*, **16**, 1176–1189.
21. Ogino,H., Ishino,S., Haugland,G. T., Birkeland,N. K., Kohda,D. and Ishino,Y. (2014) Activation of the MCM helicase from the thermophilic archaeon, *Thermoplasma acidophilum* by interactions with GINS and Cdc6-2. *Extremophiles*, **18**, 915–924.
22. Goswami,K., Arora,J. and Saha,S. (2015) Characterization of the MCM homohexamer from the thermoacidophilic euryarchaeon *Picrophilus torridus*. *Sci. Rep.*, **5**, 9057.
23. Lang,S. and Huang,L. (2015) The *Sulfolobus solfataricus* GINS Complex Stimulates DNA binding and processive DNA unwinding by minichromosome maintenance helicase. *J. Bacteriol.*, **197**, 3409–3420.

24. Sanchez-Pulido,L. and Ponting,C.P. (2011) Cdc45: the missing RecJ ortholog in eukaryotes? *Bioinformatics*, **27**, 1885–1888.
25. Persky,N.S. and Lovett,S.T. (2008) Mechanisms of recombination: lessons from *E. coli. Crit. Rev. Biochem. Mol. Biol.*, **43**, 347–370.
26. Dianov,G. and Lindahl,T. (1994) Reconstitution of the DNA base excision-repair pathway. *Curr. Biol.*, **4**, 1069–1076.
27. Burdett,V., Baitinger,C., Viswanathan,M., Lovett,S.T. and Modrich,P. (2001) *In vivo* requirement for RecJ, ExoVII, ExoI, and ExoX in methyl-directed mismatch repair. *Proc. Natl. Acad. Sci. U.S.A.*, **98**, 6765–6770.
28. Makarova,K.S., Koonin,E.V. and Kelman,Z. (2012) The CMG (CDC45/RecJ, MCM, GINS) complex is a conserved component of the DNA replication system in all archaea and eukaryotes. *Biol. Direct*, **7**, 7.
29. Li,Z., Pan,M., Santangelo,T.J., Chemnitz,W., Yuan,W., Edwards,J.L., Hurwitz,J., Reeve,J.N. and Kelman,Z. (2011) A novel DNA nuclease is stimulated by association with the GINS complex. *Nucleic Acids Res.*, **39**, 6114–6123.
30. Xu,Y., Gristwood,T., Hodgson,B., Trinidad,J.C., Albers,S.-V. and Bell,S.D. (2016) Archaeal orthologs of Cdc45 and GINS form a stable complex that stimulates the helicase activity of MCM. *Proc. Natl. Acad. Sci. U.S.A.*, **113**, 13390–13395.
31. Marinsek,N., Barry,E.R., Makarova,K.S., Dionne,I., Koonin,E.V. and Bell,S.D. (2006) GINS, a central nexus in the archaeal DNA replication fork. *EMBO Rep.*, **7**, 539–545.
32. Ogino,H., Ishino,S., Kohda,D. and Ishino,Y. (2017) The RecJ2 Protein in the thermophilic archaeon, *Thermoplasma acidophilum* is a 3′–5′ exonuclease and associates with a DNA replication complex. *J. Biol. Chem.*, **292**, 7921–7931.
33. Pan,M., Santangelo,T.J., Li,Z., Reeve,J.N. and Kelman,Z. (2011) *Thermococcus kodakarensis* encodes three MCM homologs but only one is essential. *Nucleic Acids Res.*, **39**, 9671–9680.
34. Oyama,T., Ishino,S., Fujino,S., Ogino,H., Shirai,T., Mayanagi,K., Saito,M., Nagasawa,N., Ishino,Y. and Morikawa,K. (2011) Architectures of archaeal GINS complexes, essential DNA replication initiation factors. *BMC Biol.*, **9**, 28.
35. Oyama,T., Ishino,S., Shirai,T., Yamagami,T., Nagata,M., Ogino,H., Kusunoki,M. and Ishino,Y. (2016) Atomic structure of an archaeal GAN suggests its dual roles as an exonuclease in DNA repair and a CMG component in DNA replication. *Nucleic Acids Res.*, **44**, 9505–9517.
36. Simon,A.C., Sannino,V., Costanzo,V. and Pellegrini,L. (2016) Structure of human Cdc45 and implications for CMG helicase function. *Nat. Commun.*, **7**, 11638.
37. Burkhart,B.W., Cubonova,L., Heider,M.R., Kelman,Z., Reeve,J.N. and Santangelo,T.J. (2017) The GAN exonuclease, or the flap endonuclease Fen1 and RNase HII are necessary for viability of *Thermococcus kodakarensis*. *J. Bacteriol.*, **199**, doi:10.1128/JB.00141-17.
38. Gasteiger,E., Hoogland,C., Gattiker,A., Duvaud,S., Wikins,M. R., Appel,R. D. and Bairoch,A. (2005) Protein identification and analysis tools on the ExPASy server. In: Walker,JM (ed). *The Proteomics Protocols Handbook*, Humana Press, NY, pp. 571–607.
39. Sato,T., Fukui,T., Atomi,H. and Imanaka,T. (2005) Improved and versatile transformation system allowing multiple genetic manipulations of the hyperthermophilic archaeon *Thermococcus kodakaraensis*. *Appl. Environ. Microbiol.*, **71**, 3889–3899.
40. Sato,T., Fukui,T., Atomi,H. and Imanaka,T. (2003) Targeted gene disruption by homologous recombination in the hyperthermophilic archaeon *Thermococcus kodakaraensis* KOD1. *J. Bacteriol.*, **185**, 210–220.
41. Atomi,H., Fukui,T., Kanai,T., Morikawa,M. and Imanaka,T. (2004) Description of *Thermococcus kodakaraensis* sp. nov., a well studied hyperthermophilic archaeon previously reported as *Pyrococcus* sp. KOD1. *Archaea*, **1**, 263–267.
42. Fukui,T., Atomi,H., Kanai,T., Matsumi,R., Fujiwara,S. and Imanaka,T. (2005) Complete genome sequence of the hyperthermophilic archaeon *Thermococcus kodakaraensis* KOD1 and comparison with *Pyrococcus* genomes. *Genome Res.*, **15**, 352–363.
43. Robb,F.T. and Place,A.R. (1995) Media for thermophiles. In: Robb,FT and Place,AR (eds). *Archaea: a Laboratory Manual: Thermophiles*, Cold Spring Harbor, NY, pp. 167–188.
44. Yokooji,Y., Tomita,H., Atomi,H. and Imanaka,T. (2009) Pantoate kinase and phosphopantothenate synthetase, two novel enzymes necessary for CoA biosynthesis in the Archaea. *J. Biol. Chem.*, **284**, 28137–28145.
45. Kuba,Y., Ishino,S., Yamagami,T., Tokuhara,M., Kanai,T., Fujikane,R., Daiyasu,H., Atomi,H. and Ishino,Y. (2012) Comparative analyses of the two proliferating cell nuclear antigens from the hyperthermophilic archaeon. *Genes Cells*, **17**, 923–937.
46. Bustin,S.A., Benes,V., Garson,J.A., Hellemans,J., Huggett,J., Kubista,M., Mueller,R., Nolan,T., Pfaffl,M.W., Shipley,G.L. *et al.* (2009) The MIQE guidelines: minimum information for publication of quantitative real-time PCR experiments. *Clin. Chem.*, **55**, 611–622.
47. Untergasser,A., Cutcutache,I., Koressaar,T., Ye,J., Faircloth,B.C., Remm,M. and Rozen,S.G. (2012) Primer3—new capabilities and interfaces. *Nucleic Acids Res.* **40**, e115.
48. Szambowska,A., Tessmer,I., Prus,P., Schlott,B., Pospiech,H. and Grosse,F. (2017) Cdc45-induced loading of human RPA onto single-stranded DNA. *Nucleic Acids Res.*, **45**, 3217–3230.
49. Lovett,S.T. and Kolodner,R.D. (1989) Identification and purification of a single-stranded-DNA-specific exonuclease encoded by the *recJ* gene of *Escherichia coli*. *Proc. Natl. Acad. Sci. U.S.A.*, **86**, 2627–2631.
50. Sutera,V.A. Jr, Han,E.S., Rajman,L.A. and Lovett,S.T. (1999) Mutational analysis of the RecJ exonuclease of *Escherichia coli*: identification of phosphoesterase motifs. *J. Bacteriol.*, **181**, 6098–6102.
51. Cheng,K., Xu,H., Chen,X., Wang,L., Tian,B., Zhao,Y. and Hua,Y. (2016) Structural basis for DNA 5′-end resection by RecJ. *Elife*, **5**, e14294.
52. Yuan,H., Liu,X.P., Han,Z., Allers,T., Hou,J.L. and Liu,J.H. (2013) RecJ-like protein from *Pyrococcus furiosus* has 3′-5′ exonuclease activity on RNA: implications for proofreading of 3′-mismatched RNA primers in DNA replication. *Nucleic Acids Res.*, **41**, 5817–5826.
53. Hirata,A., Kanai,T., Santangelo,T.J., Tajiri,M., Manabe,K., Reeve,J.N., Imanaka,T. and Murakami,K.S. (2008) Archaeal RNA polymerase subunits E and F are not required for transcription *in vitro*, but a *Thermococcus kodakarensis* mutant lacking subunit F is temperature-sensitive. *Mol. Microbiol.*, **70**, 623–633.
54. Courcelle,J. and Hanawalt,P.C. (1999) RecQ and RecJ process blocked replication forks prior to the resumption of replication in UV-irradiated *Escherichia coli*. *Mol. Gen. Genet.*, **262**, 543–551.
55. Lovett,S.T. and Clark,A.J. (1984) Genetic analysis of the *recJ* gene of *Escherichia coli* K-12. *J. Bacteriol.*, **157**, 190–196.
56. Cao,Z., Mueller,C.W. and Julin,D.A. (2010) Analysis of the *recJ* gene and protein from *Deinococcus radiodurans*. *DNA Repair*, **9**, 66–75.
57. Bruck,I. and Kaplan,D.L. (2013) Cdc45 protein-single-stranded DNA interaction is important for stalling the helicase during replication stress. *J. Biol. Chem.*, **288**, 7550–7563.
58. Hashimoto,Y., Puddu,F. and Costanzo,V. (2012) RAD51- and MRE11-dependent reassembly of uncoupled CMG helicase complex at collapsed replication forks. *Nat. Struct. Mol. Biol.*, **19**, 17–24.
59. Jiao,J., Wang,L., Xia,W., Li,M., Sun,H., Xu,G., Tian,B. and Hua,Y. (2012) Function and biochemical characterization of RecJ in *Deinococcus radiodurans*. *DNA Repair*, **11**, 349–356.
60. Rajman,L.A. and Lovett,S.T. (2000) A thermostable single-strand DNase from *Methanococcus jannaschii* related to the RecJ recombination and repair exonuclease from *Escherichia coli*. *J. Bacteriol.*, **182**, 607–612.